

Filling the Infrared Gap: ISO Observations of 1 Jy BL Lacertae Objects

Paolo Padovani¹, Paolo Giommi², Péter Ábrahám³, Szilárd Csizmadia³, and Attila Moór³

¹ European Southern Observatory, Karl-Schwarzschild-Str. 2, D-85748 Garching bei München, Germany
e-mail: Paolo.Padovani@eso.org

² ASI Science Data Center, ASDC, Agenzia Spaziale Italiana c/o ESRIN, Via G. Galilei, I-00044 Frascati, Italy
e-mail: paolo.giommi@asdc.asi.it

³ Konkoly Observatory, H-1525 Budapest, P.O. Box 67, Hungary
e-mail: abraham@konkoly.hu, csizmadi@konkoly.hu, moor@konkoly.hu

Received ; accepted

ABSTRACT

Aims. The large majority of BL Lacertae objects belonging to the 1 Jy sample, the class prototype for radio-selected sources, are thought to emit most of their synchrotron power in the far infrared band. Ironically, this spectral region is very sparsely sampled, with only a minority of the objects having IRAS data (most of them being upper limits or low-quality detections). We aim at filling this infrared gap by presenting new, simultaneous ISOCAM and ISOPHOT observations over the 7 – 200 μ m range (observer’s frame) for half the sample. A precise measurement of the position of the synchrotron peak frequency, ν_{peak} , can provide direct information about particle acceleration mechanisms and constrain the inverse Compton radiation that will be detected by up-coming new γ -ray missions.

Methods. We have observed seventeen 1 Jy BL Lacertae objects with the camera and the photometer on board the Infrared Space Observatory (ISO) satellite. Given the intrinsic variability of these sources, the data were taken by concatenating the pointings to ensure simultaneity. The ISOPHOT data reduction was done employing a novel correction, which mitigates the effect of chopping for faint sources.

Results. Using our new ISO data, complemented by nearly-simultaneous radio and optical observations for ten and four objects respectively, and other multi-frequency data, we have built the spectral energy distributions of our sources (plus a previously published one) and derived the rest-frame ν_{peak} . Its distribution is centered at $\sim 10^{13}$ Hz ($\sim 30\mu$ m) and is very narrow, with $\sim 60\%$ of the BL Lacs in the $1 - 3 \times 10^{13}$ Hz range. Given our set of simultaneous infrared data, these represent the best determinations available of the synchrotron peak frequencies for low-energy peaked BL Lacs. A comparison with previous such estimates, based on non-simultaneous optical and near infrared data, may indicate strong ν_{peak} variations in a number of sources, possibly associated with large flares as observed in the high-energy peaked BL Lac MKN 501.

Key words. BL Lacertae objects – Infrared: galaxies – Methods: data analysis – Radiation mechanisms: non-thermal

1. Introduction

BL Lacertae objects constitute one of the most extreme classes of active galactic nuclei (AGN), distinguished by their high luminosity, rapid variability, high ($> 3\%$) optical polarization, radio core-dominance, apparent superluminal speeds, and almost complete lack of emission lines (e.g., Urry & Padovani 1995). The broad-band emission in these objects, which extends from the radio to the gamma-ray band, appears to be dominated by non-thermal processes from the heart of the AGN, undiluted by the thermal emission present in other AGN. Therefore, BL Lacs represent the ideal class to study to further our understanding of non-thermal emission in AGN.

Synchrotron emission combined with inverse Compton scattering is generally thought to be the mechanism responsible for the production of radiation over such a wide energy range (e.g., Ghisellini et al. 1998). The frequency at which most of the synchrotron power is emitted, ν_{peak} , ranges across several orders of magnitude, going from the far-infrared to the hard X-ray band. Sources at the extremes of this wide distribution are referred to as low-energy peaked (LBL) and high-energy peaked (HBL) BL Lacs, respectively (Giommi & Padovani 1994; Padovani & Giommi 1995). Radio-selected samples include mostly objects of the LBL type, while X-ray selected samples are mostly made up of HBL.

It is ironic that the spectrum of LBL in the infrared (IR) band, where these sources’ output is thought to be largest, is

Table 1. Sample properties.

Name	RA(J2000)	Dec(J2000)	z	$\langle R_{\text{mag}} \rangle$	$F_{5\text{GHz}}$ Jy
PKS 0048–097	00 50 41.3	–09 29 06	>0.2	16.5	2.0
PKS 0118–272	01 20 31.7	–27 01 24	>0.559	17.0	1.1
PKS 0138–097	01 41 25.8	–09 28 44	0.733	17.0	1.2
PKS 0426–380	04 28 40.4	–37 56 19	1.110	18.0	1.2
S5 0454+844	05 08 42.4	+84 32 05	>1.340	19.0	1.4
PKS 0537–441	05 38 50.4	–44 05 09	0.896	13.5	4.0
PKS 0735+178	07 38 07.1	+17 42 27	>0.424	14.5	2.0
PKS 1144–379	11 47 01.4	–38 12 10	1.048	16.5	1.6
OQ 530	14 19 46.6	+54 23 15	0.152	14.5	1.1
PKS 1519–273	15 22 37.7	–27 30 10	>0.2	18.5	2.4
PKS 1749+701	17 48 32.8	+70 05 51	0.770	16.5	1.1
PKS 1749+096	17 51 32.8	+09 39 01	0.320	15.5	1.9
S5 1803+784	18 00 45.7	+78 28 04	0.684	16.5	2.6
4C 56.27	18 24 07.2	+56 51 00	0.664	18.5	1.7
PKS 2131–021	21 34 10.3	–01 53 17	1.285	20.0	2.1
PKS 2240–260	22 43 26.4	–25 44 31	0.774	17.5	1.0
PKS 2254+074	22 57 17.3	+07 43 12	0.190	17.0	1.2

very sparsely known (e.g., Sambruna et al. 1996; Giommi et al. 2002; Massaro et al. 2005). IR data for the 1 Jy, the prototype radio-selected BL Lac sample are, for example, very sparse. The purpose of this paper is to remedy this situation by presenting ISOCAM and ISOPHOT observations of 1 Jy BL Lacs covering the $6.7 - 200\mu\text{m}$ range. Since $\nu_{\text{peak}} \propto \gamma_{\text{peak}}^2 \delta B$, where γ_{peak} is the Lorentz factor of the electrons emitting most of the radiation, δ is the Doppler factor, and B is the strength of the magnetic field, its precise measurement can provide direct information about particle acceleration mechanisms. The position of ν_{peak} is also important for the up-coming Astro-rivelatore Gamma a Immagini Leggero (AGILE¹) and Gamma ray Large Area Space Telescope (GLAST²) missions, as they will sample the γ -ray band close to the peak of the inverse Compton emission from LBL and flat-spectrum radio quasars, whose location depends on that of the synchrotron one.

In Sect. 2 we present our sample, Sect. 3 discusses the Infrared Space Observatory (ISO) observations, data analysis, and results, while in Sect. 4 we derive the spectral energy distributions and ν_{peak} values. Finally, Sect. 5 summarizes our conclusions. Throughout this paper spectral indices are written $S_\nu \propto \nu^{-\alpha}$.

2. The sample

The 1 Jy sample of BL Lacs is the only sizeable, complete sample of radio bright BL Lacs. It includes 34 objects with radio flux > 1 Jy at 5 GHz (Stickel et al. 1991). All 1 Jy BL Lacs have been studied in detail in the radio and optical bands; all objects have also soft X-ray data, primarily from ROSAT (Urry et al. 1996). Most of the sources have also been detected by the Wilkinson Microwave Anisotropy Probe (WMAP) satellite (Bennett et al. 2003) and about 40% of them have also hard

X-ray (*BeppoSAX*) data (e.g., Padovani et al. 2004 and references therein). In the IR band, on the other hand, 1 Jy BL Lacs are not very well studied. For example, only $\sim 40\%$ of 1 Jy BL Lacs have IRAS data, and many of these are of low quality or only upper limits. We selected for ISO observations all 1 Jy BL Lacs visible by the satellite and not already part of other programs. This included seventeen 1 Jy BL Lacs (or 50% of the sample). All sources are LBL. The object list and basic characteristics are given in Tab. 1. Accurate radio positions and redshifts come from the NASA/IPAC Extragalactic Database (NED), mean R magnitudes are from Heidt & Wagner (1996), while 5 GHz radio fluxes are from Stickel et al. (1991).

3. Observations, data analysis, and results

The ISO satellite (Kessler et al. 1996) was equipped with a 60 cm Ritchey-Chrétien telescope and had four instruments. For our observations we used the camera (ISOCAM) and the photometer (ISOPHOT). Given the intrinsic variability of BL Lacs, we needed to observe each object at a single epoch. Thus, the three different Astronomical Observation Templates (AOTs) we used (see below) were concatenated in order to warrant as much simultaneity as possible for the measurements.

3.1. ISOCAM

All sources were observed with the 32×32 pixel ISOCAM (Blommaert et al. 2003) in staring mode (AOT = CAM01) using the long-wavelength (LW) detector in three different bands: LW2 ($\lambda = 6.7\mu\text{m}$), LW7 ($\lambda = 9.6\mu\text{m}$), and LW3 ($\lambda = 14.3\mu\text{m}$). The pixel scale was $6''$ and the total field of view 196×196 arcsec². The total exposure times were computed as $T_{\text{int}} \times N_{\text{exp}}$, where $T_{\text{exp}} = 2.1$ s is the integration time of a single exposure and N_{exp} is the number of exposures. Typical exposure times are 100 s, 100 s, and 75 s for the LW2, LW7, and LW3 filters, re-

¹ <http://agile.rm.iasf.cnr.it/>

² <http://glast.gsfc.nasa.gov/>

Table 2. ISO journal of observations.

Name	ISO_id CAM/P2/C100&C200	Observing date
PKS 0048–097	38701401/02/03	1996 Dec 8
PKS 0118–272	74400104/05/06	1997 Nov 28
PKS 0138–097	76301007/08/09	1997 Dec 17
PKS 0426–380	69702410/11/12	1997 Oct 12
S5 0454+844	68700413/14/15	1997 Oct 2
PKS 0537–441	70201116/17/18	1997 Oct 18
PKS 0735+178	72301882/83/84	1997 Nov 8
PKS 1144–379	25400637/38/39	1996 Jul 27
OQ 530	40200746/47/48	1996 Dec 22
PKS 1519–273	43401152/53/54	1997 Jan 23
PKS 1749+701	39901458/59/60	1996 Dec 19
PKS 1749+096	82200287/88/89	1998 Feb 14
S5 1803+784	15100861/62/63	1996 Apr 16
4C 56.27	15100964/65/66	1996 Apr 16
PKS 2131–021	38601073/74/75	1996 Dec 6
PKS 2240–260	16402576/77/78	1996 Apr 29
PKS 2254+074	37900579/80/81	1996 Nov 29

spectively. A journal of the observations is presented in Tab. 2, which gives the name of the source, the corresponding ISO_id which uniquely identifies an ISO observation, and the observing date.

The data analysis was performed with the ISOCAM Interactive Analysis (CIA; Ott et al. 1997) tool, Ver. 5.0. The default steps of CIA were used for dark current subtraction, removal of cosmic ray hits (glitches), exposure co-addition, flat fielding, and flux conversion to astronomical units³. The transient correction we adopted was not the standard one but that based on the Fouks-Schubert model (Fouks & Schubert 1995) which is valid for low contrasted ISOCAM LW observations (Coulais & Abergel 2000). This was necessary since our LW observations were preceded by short-wavelength (SW) measurements (which could not be used), which made more difficult to get the history of the LW detector.

The source flux was derived by performing aperture photometry with a radius which contained $\sim 90\%$ of the flux for each filter, namely 2 pixels for LW2, 3 pixels for LW7, and 4 pixels for LW3, correcting for the missing flux using the CIA point spread function (PSF) library. The background was derived in a four pixel wide annulus whose inner radius was two pixels larger than the extraction radius for most sources (see below). The aperture centre was determined in an iterative way by first placing it on the brightest pixel and then by moving it in 1/4 pixel steps around that position until the largest value was reached. The flux uncertainty was estimated by adding in quadrature the root mean squared (rms) of the image within the extraction radius and the 1σ uncertainty of the background estimate. Systematic errors of ISOCAM photometry are $\sim 15\%$

³ This last step assumes $f_\nu \propto \nu^{-1}$, which is the average spectrum of our sources (see below), so no colour-correction was applied (in the most extreme case, $f_\nu \propto \nu^{-2.7}$, this would have been $\sim 4\%$, way below our uncertainties).

Table 3. ISOCAM fluxes^a and slopes.

Name	LW2 [6.7 μ m]	LW7 [9.6 μ m]	LW3 [14.3 μ m]	α_ν
PKS 0048–097	18.2 \pm 2.0	19.2 \pm 6.8	25.7 \pm 5.7	0.4 \pm 0.4
PKS 0118–272	18.2 \pm 2.7	20.1 \pm 7.3	35.7 \pm 5.6	0.9 \pm 0.3
PKS 0138–097	9.1 \pm 2.2	11.9 \pm 5.5	18.9 \pm 5.2	1.0 \pm 0.6
PKS 0426–380	2.5 \pm 1.2	<14.7	19.0 \pm 5.6	2.7 \pm 0.7
S5 0454+844	5.5 \pm 2.2	<16.2	13.5 \pm 5.7	1.2 \pm 0.9
PKS 0537–441	18.4 \pm 2.0	29.1 \pm 5.5	32.6 \pm 5.3	0.8 \pm 0.2
PKS 0735+178	19.3 \pm 2.0	23.2 \pm 6.4	33.4 \pm 5.1	0.7 \pm 0.3
PKS 1144–379	10.7 \pm 1.7	14.4 \pm 6.2	37.2 \pm 5.7	1.6 \pm 0.3
OQ 530	21.0 \pm 2.6	32.8 \pm 5.3	44.1 \pm 5.2	1.0 \pm 0.2
PKS 1519–273	9.9 \pm 2.9	11.2 \pm 6.4	<14.1	0.4 \pm 1.6
PKS 1749+701	29.2 \pm 2.5	46.7 \pm 6.6	54.3 \pm 5.5	0.8 \pm 0.2
PKS 1749+096	33.2 \pm 2.4	43.0 \pm 7.3	68.8 \pm 6.2	1.0 \pm 0.2
S5 1803+784	29.3 \pm 2.0	33.0 \pm 5.7	66.8 \pm 5.1	1.1 \pm 0.1
4C 56.27	6.1 \pm 2.2	8.8 \pm 3.7	9.2 \pm 3.7	0.5 \pm 0.6
PKS 2131–021	12.1 \pm 2.3	<17.6	10.7 \pm 4.3	–0.2 \pm 0.5
PKS 2240–260	6.9 \pm 2.1	21.6 \pm 5.9	17.8 \pm 5.3	1.2 \pm 0.5
PKS 2254+074	14.1 \pm 2.3	17.8 \pm 6.1	30.5 \pm 5.7	1.0 \pm 0.4

^amJy

for point sources (Blommaert et al. 2003), which are typically below our uncertainties.

3.1.1. Notes on individual sources

PKS 0138–097: faint source with a stronger source ~ 6.5 pixels away in the LW2 image; we then estimated the background in a two (instead of four) pixel wide annulus.

PKS 0426–380: faint source; to increase the signal to noise (S/N) we used an extraction radius of 1 pixel for the LW2 filter, instead of our default value of two. No significant detection in the LW7 filter.

S5 0454+844: faint source with another source of comparable flux ~ 8 pixels away in the LW2 image; we then estimated the background in a three (instead of four) pixel wide annulus. No significant detection in the LW7 filter. Faint source with another source of comparable flux ~ 8 pixels away in the LW3 image; we then estimated the background in a four pixel wide annulus just outside the extraction circle.

PKS 0735+178: another source of comparable flux ~ 5.5 pixels away in the LW7 image; we then estimated the background in a four pixel wide annulus whose inner radius was four (instead of two) pixels larger than the extraction radius. Same for the LW3 filter (another source ~ 6.5 pixels away).

PKS 1519–273: another source of comparable flux ~ 7.5 pixels away in the LW7 image; we then estimated the background in a two (instead of four) pixel wide annulus. No significant detection in the LW3 filter.

PKS 1749+701: structure in the background of the LW3 image; we then estimated the background in a region closer to the source (inner radius was one pixel larger than the extraction radius and annulus was three pixels wide).

4C 56.27: faint source; to increase the signal to noise (S/N) we used an extraction radius of three pixels for the LW3 filter, instead of four.

PKS 2131–021: faint source; no significant detection in the LW7 filter. To increase the signal to noise (S/N) we used an extraction radius of three pixels for the LW3 filter, instead of four.

PKS 2240–260: structure in the background of the LW2 image; we then estimated the background in a region closer to the source (inner radius was one pixel larger than the extraction radius).

3.2. ISOPHOT

All sources were observed with ISOPHOT (Laureijs et al. 2003) in rectangular chopped mode, i.e., the line-of-sight was switched periodically between the source and the background position, the latter being placed at $180''$ from the source. For each source, data were taken with the P2 detector at $25\mu\text{m}$, with the C100 detector at 65, 80 and $100\mu\text{m}$, and with the C200 detector in the 120, 170 and $180\mu\text{m}$ bands. Typical on-source exposure times were 128 s (P2), 32–64 s (C100), and 32 s (C200). A journal of the observations is presented in Tab. 2, which gives the name of the source, the corresponding ISO_id, and the observing date.

The data reduction was performed using the ISOPHOT Interactive Analysis Software Package V10.0 (PIA, Gabriel et al. 1998). After corrections for non-linearities of the integration ramps, an 8-point signal pattern was created from each observation by overplotting and averaging the basic blocks of the observation (the repeated background+source cycles; for details see Ábrahám et al. 2003). The signals of the patterns were transformed to a standard reset interval of 1/4 s, and an orbital dependent dark current was subtracted. The signals were corrected for non-linearities of the detectors by applying signal linearization corrections. From the patterns a (source – background) difference signal was then extracted. In most cases the measured difference signal underestimates the real signal due to short term detector transients. Therefore, we applied the signal loss correction algorithm as implemented in PIA. This correction is a function of the chopping frequency and the measured difference signal. The flux calibration of the C100/C200 measurements was performed by comparison with the on-board fine calibration source (FCS), which was also measured in chopped mode. At $25\mu\text{m}$ the detector’s actual sensitivity could be reliably predicted from the orbital position of the observation, and an orbital dependent default responsivity was applied. Finally, the derived flux densities were corrected for the finite size of the aperture by using the standard correction values.

In a chopped observation the slow detector baseline variations are expected to be cancelled via the frequent alternation of the source and background positions. In the case of very faint sources, however, the time per chopper plateau was often rather long, and in many cases only two ON-OFF cycles were performed. In these observations the baseline variations may not be perfectly corrected via the chopping procedure, since the temporal evolution of the baseline was only scarcely sampled. From a comprehensive calibration study we found that in the case of P2 observations of faint sources with only two chopper cycles the resulting fluxes were incorrect, usually overestimat-

ing the true value. In order to cancel the signal transient, we introduced a new correction at the beginning of the processing scheme, by applying a transient correction developed for staring (rather than chopped) P2 observations.

The staring transient correction normally works on signals at the Signal per Ramp Data (SRD) level, but in the case of a chopped observation it has to be applied before the pattern is created. Thus we modified the PIA procedure “process_erd_to_pattern.pro” and applied the transient correction on each pair-wise signal before pattern creation. The agreement with the fluxes predicted by extrapolating the ISOCAM fluxes was significantly improved with the new correction. We applied this algorithm to all our P2 observations which had only two ON-OFF cycles. We then processed further the measurements as normal chopped observations. Notice that some residual problems with uncorrected P2 data might remain (see § 4.2.1).

The flux uncertainty at $25\mu\text{m}$ was estimated to be of the order of 50 mJy at faint flux levels. For the C100/C200 filters one important source of systematic uncertainty may be related to the signal loss correction. In addition, the actual responsivity of the detector had to be derived from the accompanying FCS measurement, thereby introducing an additional uncertainty factor. Finally, at long wavelengths ($\lambda \geq 100\mu\text{m}$) sky confusion noise can be the dominant source of photometric error.

Note that for the four sources for which ISOCAM detected a close-by, relatively strong source, namely PKS 0138–097, S5 0454+844, PKS 0735+178, and PKS 1519–273, some confusion is expected in the ISOPHOT band (see § 4.2.1).

3.3. Results

Our ISOCAM fluxes are reported in Tab. 3. When no significant detection was obtained we give 3σ upper limits. Tab. 3 gives also the best fit spectral slopes (in frequency space) to the ISOCAM data. These were derived by taking into account the errors on the fluxes and by excluding non detections. The mean value is $\langle\alpha_\nu\rangle = 0.95 \pm 0.15$ (median 1.0), while the weighted mean is $\langle\alpha_\nu\rangle = 0.99 \pm 0.06$. This is consistent with expectations, as a synchrotron peak frequency in the IR means $\nu f_\nu \approx \text{const}$ in the ISO bands, and therefore $f_\nu \propto \nu^{-1}$, as indeed observed.

Our ISOPHOT fluxes are reported in Tab. 4. When no significant detection was obtained, or the formal uncertainty was larger than the measured flux density value, 3σ upper limits are given.

4. Discussion

4.1. Host galaxy contribution to the IR flux

Before studying the spectral energy distributions (SEDs) of our sources it is important to assess a possible contribution from the galaxy which hosts the BL Lac. To this aim, we estimated the host galaxy flux in the IR band, following the approach of Bertone et al. (2000). A literature search actually revealed that 13 out of our 17 BL Lacs are optically unresolved, that is no host galaxy is detected (Pursimo et al. 2002; Sbaruffati

Table 4. ISOPHOT fluxes^a.

Name	$P2/25$ [25 μm]	$C100/C_{.50}$ [65 μm]	$C100/C_{.70}$ [80 μm]	$C100/C_{.100}$ [100 μm]	$C200/C_{.120}$ [120 μm]	$C200/C_{.160}$ [170 μm]	$C200/C_{.180}$ [180 μm]
PKS 0048–097	195 \pm 48	218 \pm 115	<552	<378	<1032	<1377	< 933
PKS 0118–272	53 \pm 48	196 \pm 69	290 \pm 174	150 \pm 132	< 948	331 \pm 249	< 822
PKS 0138–097	199 \pm 48	317 \pm 76	271 \pm 65	<549	<1089	<1524	< 981
PKS 0426–380	63 \pm 48	126 \pm 60	<819	<180	< 792	400 \pm 201	< 762
S5 0454+844	<144	<375	<783	<582	<1746	<3771	<6423
PKS 0537–441	70 \pm 48	249 \pm 60	155 \pm 117	<180	365 \pm 315	404 \pm 387	< 933
PKS 0735+178	225 \pm 48	221 \pm 133	<366	523 \pm 167	<1197	< 975	<1029
PKS 1144–379	115 \pm 48	269 \pm 75	259 \pm 61	<309	<1353	<1566	<1857
OQ 530	139 \pm 48	160 \pm 97	183 \pm 60	204 \pm 181	< 837	351 \pm 237	337 \pm 251
PKS 1519–273	249 \pm 48	312 \pm 77	164 \pm 60	137 \pm 115	<1305	<4215	<5025
PKS 1749+701	132 \pm 48	<285	76 \pm 60	247 \pm 60	< 846	<2307	<1725
PKS 1749+096	134 \pm 48	503 \pm 75	619 \pm 93	346 \pm 102	<1347	<3495	<4146
S5 1803+784	162 \pm 48	75 \pm 60	330 \pm 274	312 \pm 60	410 \pm 305	472 \pm 278	507 \pm 300
4C 56.27	63 \pm 48	712 \pm 144	<429	<411	<1182	<1914	459 \pm 416
PKS 2131–021	178 \pm 48	<189	<282	170 \pm 60	<1017	< 927	387 \pm 331
PKS 2240–260	139 \pm 48	<195	<213	198 \pm 60	< 909	<1146	<1122
PKS 2254+074	190 \pm 48	114 \pm 96	379 \pm 115	265 \pm 185	<1017	<1104	<1134

^amJy

et al. 2005). For the remaining four sources, we found host galaxy R magnitudes in Pursimo et al. (2002) and converted them to B magnitudes using the evolutionary synthesis model of Dunlop et al. (1989). We then used the results of Mazzei & DeZotti (1994), who calculated the flux ratio between the IRAS and the B bands for a sample of 47 ellipticals, to estimate the galaxy contributions at 12, 25, 60, and 100 μm . These turned out to be *extremely* low. The maximum expected contributions in fact, were around 1%, 0.01%, 0.1%, and 0.2% of the observed fluxes at 12, 25, 60, and 100 μm respectively. We thus conclude that for the BL Lacs in our sample the contribution of the host galaxy to their ISO flux is completely negligible.

4.2. Spectral energy distributions

To constrain the synchrotron power peak and to address the relevance of our ISO data in terms of emission processes in BL Lacs, we have assembled multifrequency data for all our sources. We have also included S5 2007+777, a 1 Jy BL Lac at $z = 0.342$ with previously published ISOPHOT data (Peng et al. 2000). Since we are not interested in characterizing the inverse Compton emission, we limited ourselves to frequencies $\leq 10^{16}$ Hz. The main source of information was NED. Additional data were taken from the WMAP catalogue (Bennett et al. 2003), the Two Micron All Sky Survey (2MASS) (Cutri et al. 2000), the Guide Star Catalogue II⁴, and the Sloan Digital Sky Survey (SDSS). Therefore, most data are not simultaneous with our observations. For more than half of our sources, however, we were able to find nearly-simultaneous (typically within a month) radio observations in the University of Michigan Radio Astronomy Observatory (UMRAO) database⁵. These are re-

ported in Table 5. Furthermore, nearly-simultaneous optical data were available for PKS 0735+178 (Bai et al. 1999), OQ 530 (Massaro et al. 2004), and S5 1803+784 (Nesci et al. 2002). As regards S5 2007+777, Peng et al. (2000) published simultaneous radio (seven frequencies), ISOPHOT (60 and 100 μm), and optical (R band) observations of this object.

The SEDs for our sources are shown in Fig. 1, where bigger, darker symbols and upper limits indicate ISO data and the nearly-simultaneous radio and optical data, and smaller, lighter symbols represent non-simultaneous data collected from the literature.

4.2.1. Synchrotron peak frequencies

We determined ν_{peak} for our sources by applying an homogeneous synchrotron – inverse self-Compton (SSC) model in the $\log \nu - \log \nu f_{\nu}$ plane to the SEDs. The SSC model was adapted from Tavecchio et al. (1998) and assumes that radiation is produced by a population of relativistic electrons emitting synchrotron radiation in a single zone of a jet that is moving at relativistic speed and at a small angle to the line of sight (see Giommi et al. 2002 and Padovani et al. 2003 for previous applications of this model and more details). Padovani et al. (2003) make the point that, despite the fact that we cannot fully constrain the model parameters, ν_{peak} , a combination of magnetic field strength, Doppler factor, and electron break energy, is relatively well constrained even for relatively large variations of these parameters, which affect more strongly the high-energy/inverse Compton part of the SED.

Some previous papers have derived ν_{peak} by fitting analytical functions, such as a parabola or a third-degree polynomial, to the SED of blazars (e.g., Sambruna et al. 1996; Fossati et al. 1998). We believe that our approach, although more complex and time consuming, is more robust especially when deal-

⁴ <http://archive.stsci.edu/gsc/>

⁵ The Bologna group has also performed a radio monitoring of some of our sources (Venturi et al. 2001). The UMRAO observations, however, were always closer in time to our observing dates.

Table 5. Nearly-simultaneous radio observations.

Name	F _{4.8GHz} (Jy)	Observing date	F _{8.0GHz} (Jy)	Observing date	F _{14.5GHz} (Jy)	Observing date
PKS 0048–097	1.58 ± 0.06	1996 Dec 13	1.96 ± 0.03	1996 Dec 9	2.12 ± 0.05	1996 Dec 11
PKS 0735+178	1.06 ± 0.04	1997 Dec 2	0.69 ± 0.16	1997 Nov 24	0.94 ± 0.11	1997 Dec 10
OQ 530	0.56 ± 0.15	1997 Jan 6	0.64 ± 0.03	1996 Dec 30
PKS 1749+701	0.63 ± 0.04	1996 Dec 13	0.86 ± 0.03	1996 Dec 19
PKS 1749+096	2.26 ± 0.03	1998 Feb 18	3.40 ± 0.08	1998 Feb 17	4.02 ± 0.09	1998 Feb 4
S5 1803+784	2.91 ± 0.04	1996 Apr 3	2.90 ± 0.19	1996 Apr 23	3.18 ± 0.06	1996 Apr 11
4C 56.27	1.79 ± 0.04	1996 Apr 16	2.34 ± 0.06	1996 Apr 24
PKS 2131–021	1.67 ± 0.02	1997 Jan 6	1.56 ± 0.04	1996 Dec 19
PKS 2254+074	0.48 ± 0.02	1996 Dec 19

ing with sparsely sampled SEDs, as we are guided by physics rather than just analytical fitting.

During our fitting procedure we adhered to the following guidelines: 1. more weight was given to our nearly-simultaneous data; 2. more weight was given to ISOCAM data, which have smaller error bars; 3. clear outliers were not taken into account; in case of ISOPHOT data, these indicate confusion (see § 3.2) and/or some residual calibration issues; 4. only data points with $\nu \gtrsim 3 \times 10^9$ Hz were included. Our derived rest-frame ν_{peak} values are given in Tab. 6. Based on our experience, we believe that most of our values are determined to better than 0.5 dex. Exceptions to this rule include PKS 1519–273, PKS 2131–021, and PKS 2254+074, whose SEDs are sparse and/or whose ISO continuum shape is somewhat irregular (see Fig. 1).

The ν_{peak} distribution is very narrow, with 10/18 sources having values in the range $1 - 3 \times 10^{13}$ Hz. The mean value is $\langle \log \nu_{\text{peak}} \rangle = 13.0 \pm 0.1$ (median 13.0), that is $\sim 30 \mu\text{m}$. Given our set of simultaneous IR data, these represent the best determinations available of the synchrotron peak frequencies for the 1 Jy BL Lac sample.

4.2.2. Synchrotron peak variability in IR band

Inspection of Fig. 1 shows that quite a few of our sources have a nearly-simultaneous SED around the peak which is quite different from the one previously available using non-simultaneous data from the literature. The most obvious cases include PKS 0048–097, PKS 0537–441, PKS 0735+178, OQ 530, 4C 56.27, where ν_{peak} could have changed by over one order of magnitude. This impression is confirmed by a comparison with the ν_{peak} values derived by Sambruna et al. (1996) for these objects, which are larger than ours by factors ~ 20 , 120, 10, 2, and 8 respectively. This may be indicative of large changes in the location of the synchrotron peak, as observed in the case of the high-energy peaked BL Lac MKN 501 (e.g., Pian et al. 1998; Massaro et al. 2006). Alternatively, ν_{peak} could have stayed constant, and the large optical variability would be due to a shift in normalization of the whole SED, implying a correspondingly high change in the IR flux. Simultaneous optical-IR monitoring is required to be able to distinguish between the two possibilities.

Table 6. Rest-frame synchrotron peak frequencies and wavelengths.

Name	ν_{peak} 10^{13} Hz	λ_{peak} μm
PKS 0048–097	0.3	100
PKS 0118–272	10	3
PKS 0138–097	0.3	100
PKS 0426–380	0.5	60
S5 0454+844	0.5	60
PKS 0537–441	0.1	300
PKS 0735+178	1	30
PKS 1144–379	1	30
OQ 530	3	10
PKS 1519–273	1	30
PKS 1749+701	3	10
PKS 1749+096	0.3	100
S5 1803+784	1	30
4C 56.27	0.5	60
S5 2007+777 ^a	1	30
PKS 2131–021	2	15
PKS 2240–260	2	15
PKS 2254+074	2	15

^aISOPHOT data published by Peng et al. (2000).

4.3. Astrophysical relevance

A precise measurement of ν_{peak} can obviously characterize synchrotron emission from blazars. Furthermore, its value and that of the spectral curvature around the maximum emission can constrain particle acceleration mechanisms in these sources (e.g., Massaro et al. 2006). This is also extremely relevant for two up-coming γ -ray missions, that is AGILE and GLAST. These observatories, in fact, will sample inverse Compton emission above the peak for LBL and flat-spectrum radio quasars. Moreover, the large synchrotron peak variability possibly present in a few of our sources will also be important to constrain the link between the two main emission processes in blazars and the source of the inverse Compton seed photons (e.g., Sokolov et al. 2004).

4.4. Previous ISO observations of BL Lacs

To the best of our knowledge, only three ISO observations of BL Lacs have been published. Beside the already mentioned

S5 2007+777, these include PKS 2155–304 (ISOCAM and ISOPHOT; Bertone et al. 2000) and Mrk 180 (ISOPHOT, one detection at $90\mu\text{m}$; Anton et al. 2004), both of the HBL type.

5. Conclusions

We have presented new, simultaneous ISOCAM and ISOPHOT observations covering the $7\text{--}200\mu\text{m}$ range for seventeen (out of 34) BL Lacertae objects belonging to the 1 Jy sample, the prototype radio-selected (low-energy peaked) sample. These data open up a new window on the spectral energy distributions of low-energy peaked BL Lacs and fill a glaring gap in their far-infrared spectra. They also represent a sevenfold (eighteenfold) increase in the number of published ISO results for BL Lacs (LBL).

Our main results can be summarized as follows:

1. Our detection rate is good: 100%, 82%, and 94% at 6.7 (LW2), 9.6 (LW7), and 14.3 (LW3) μm (ISOCAM), and 94%, $\sim 65\%$, and $\sim 20\%$ at 25 (P2), 65 – 100 (C100), and 120 – 180 (C200) μm (ISOPHOT) respectively. To deal with the effect of chopping on our relatively faint sources, which would lead to a flux overestimate at 25 μm , we have also employed a novel correction in the ISOPHOT data reduction;
2. We have built the spectral energy distributions of our sources, with the addition of a previously published one, by using our new ISO data, complemented by nearly-simultaneous radio data for about half the sample (and optical data for four sources), and other non-simultaneous multi-frequency data. We have then derived the synchrotron peak frequency, ν_{peak} . This turned out to have a very narrow distribution, with $\sim 60\%$ of the sources having values in the range $1 - 3 \times 10^{13}$ Hz, centered at $\sim 10^{13}$ Hz ($\sim 30\mu\text{m}$). These represent the best determinations available of the synchrotron peak frequencies for low-energy peaked BL Lacs;
3. A comparison with previous such estimates, based on non-simultaneous optical and near infrared data, may indicate strong ν_{peak} variations in a number of sources, possibly associated with large flares as observed in the high-energy peaked BL Lac MKN 501.

These results, apart from characterizing synchrotron emission in blazars, can constrain particle acceleration mechanisms and are also important for the planning and data interpretation of up-coming new γ -ray missions.

Acknowledgements. PP thanks the European Space Astronomy Centre (ESAC; formerly known as VILSPA) for its hospitality at the start of the data reduction process, Rosario Lorente for her expert ISOCAM assistance, and Piero Rosati for IDL help. We acknowledge the support of Paul Barr, Tommaso Maccacaro, Gianpiero Tagliaferri, and Anna Wolter at an early stage of this project. The ISOCAM data presented in this paper were analysed using CIA, a joint development by the ESA Astrophysics Division and the ISOCAM Consortium. The ISOCAM Consortium is led by the ISOCAM PI, C. Cesarsky. The ISOPHOT data presented in this paper were reduced using PIA, which is a joint development by the ESA Astrophysics

Division and the ISOPHOT consortium, with the collaboration of the Infrared Analysis and Processing Center (IPAC) and the Instituto de Astrofísica de Canarias (IAC). This research has made use of data from the University of Michigan Radio Astronomy Observatory which is supported by funds from the University of Michigan, of the NASA/IPAC Extragalactic Database (NED), which is operated by the Jet Propulsion Laboratory, California Institute of Technology, under contract with the National Aeronautics and Space Administration, of data products from the Two Micron All Sky Survey, which is a joint project of the University of Massachusetts and the Infrared Processing and Analysis Center/California Institute of Technology, funded by the National Aeronautics and Space Administration and the National Science Foundation, of Guide Star Catalogue II data, and of Sloan Digital Sky Survey (SDSS) data. Funding for the SDSS and SDSS-II has been provided by the Alfred P. Sloan Foundation, the Participating Institutions, the National Science Foundation, the U.S. Department of Energy, the National Aeronautics and Space Administration, the Japanese Monbukagakusho, the Max Planck Society, and the Higher Education Funding Council for England. The SDSS Web Site is <http://www.sdss.org/>.

References

- Ábrahám, P., Acosta-Pulido, J. A., Klaas, U., Bianchi, S., Radovich, M., & Schmidtobreick, L. 2003, The calibration legacy of the ISO Mission, ESA SP-481, 89
- Antón, S., Browne, I. W. A., Marchã, M. J. M., Bondi, M., Polatidis, A. 2004, MNRAS, 352, 673
- Bai, J. M., Xie, G. Z., Li, K. H., Zhang, X., & Liu, W. W. 1999, A&AS, 136, 455
- Bennett, C. L., Hill, R. S., Hinshaw, G. et al. 2003, ApJS, 148, 97
- Bertone, E., Tagliaferri, G., Ghisellini, G., Treves, A., Barr, P., Celotti, A., Chiaberge, M., & Maraschi, L. 2000, A&A, 356, 1
- Blommaert, J., Siebenmorgen, R., Coulais, A., et al. 2003, The ISO Handbook, CAM - The ISO Camera, ESA SP-1262, Vol. II
- Coulais, A., & Abergel, A. 2000, A&AS, 141, 533
- Cutri, R. M., et al. 2000, Explanatory Supplement to the 2MASS Second Incremental Data Release, available at: <http://www.ipac.caltech.edu/2mass/releases/second/doc/explsup.pdf>
- Dunlop, J. S., Guiderdoni, B., Rocca-Volmerange, B., Peacock, J. A., & Longair, M. S. 1989, MNRAS, 240, 257
- Fossati, G., Maraschi, L., Celotti, A., Comastri, A., & Ghisellini, G. 1998, MNRAS, 299, 433
- Fouks, B. I., & Schubert, J. 1995, SPIE, 2475, 487
- Gabriel, C., Acosta-Pulido, J., & Heinrichsen, I. 1998, ASP Conf. Ser. 145, Astronomical Data Analysis Software and Systems VII, 7, 165
- Ghisellini, G., Celotti, A., Fossati, G., Maraschi, L., & Comastri, A. 1998, MNRAS, 301, 451
- Giommi, P., Capalbi, M., Fiocchi, M., Memola, E., Perri, M., Piranomonte, S., Rebecchi, S., & Massaro, E. 2002, Blazar Astrophysics with BeppoSAX and Other Observatories, 63
- Giommi, P., & Padovani, P. 1994, MNRAS, 268, L51
- Heidt, J., & Wagner, S. J. 1996, A&A, 305, 42
- Kessler, M. F., Steinz, J. A., Andereg, M. E., et al. 1996, A&A, 315, L27
- Laureijs, R. J., Klaas, U., Richards, P. J., et al. 2003, The ISO Handbook, PHT - The Imaging Photo-Polarimeter, ESA SP-1262, Vol. IV
- Massaro, E., Mantovani, F., Fanti, R., Maesano, M., Montagni, F., Nesci, R., Sclavi, S., Tosti, G., & Venturi, T. 2004, A&A, 423, 935

- Massaro, E., Sclavi, S., Giommi, P., Perri, M., & Piranomonte, S. 2005, *Multifrequency Catalogue of Blazars* (Aracne, Rome)
- Massaro, E., Tramacere, A., Perri, M., Giommi, P., & Tosti, G. 2006, *A&A*, 448, 861
- Mazzei, P., & DeZotti, G. 1994, *ApJ*, 426, 97
- Nesci, R., Massaro, E., Maesano, M., Montagni, F., Sclavi, S., Venturi, T., Dallacasa, D., & D'Alessio, F. 2002, *AJ*, 124, 53
- Ott, S., Abergel, A., Altieri, B., et al. 1997, *ASP Conf. Ser.* 125, *Astronomical Data Analysis Software and Systems VI*, 6, 34
- Padovani, P., Costamante, L., Giommi, P., Ghisellini, G., Celotti, A., & Wolter, A. 2004, *MNRAS*, 347, 1282
- Padovani, P., & Giommi, P. 1995, *ApJ*, 444, 567
- Padovani, P., Perlman, E. S., Landt, H., Giommi, P., & Perri, M. 2003, *ApJ*, 588, 128
- Peng, B., Kraus, A., Krichbaum, T. P., et al. 2000, *A&A*, 353, 937
- Pian, E., Vacanti, G., Tagliaferri, G., et al. 1998, *ApJ*, 492, L17
- Pursimo, T., Nilsson, K., Takalo, L. O., Sillanpää, A., Heidt, J., & Pietilä, H. 2002, *A&A*, 381, 810
- Sambruna, R. M., Maraschi, L., & Urry, C. M. 1996, *ApJ*, 463, 444
- Sbarufatti, B., Treves, A., & Falomo, R. 2005, *ApJ*, 635, 173
- Sokolov, A., Marscher, A. P., & McHardy, I. M. 2004, *ApJ*, 613, 725
- Stickel, M., Padovani, P., Urry, C. M., Fried, J. W., & Kühr, H. 1991, *ApJ*, 374, 431
- Tavecchio, F., Maraschi, L., & Ghisellini, G. 1998, *ApJ*, 509, 608
- Urry, C. M., & Padovani, P. 1995, *PASP*, 107, 803
- Urry, C. M., Sambruna, R. M., Worrall, D. M., Kollgaard, R. I., Feigelson, E. D., Perlman, E. S., & Stocke, J. T. 1996, *ApJ*, 463, 424
- Venturi, T., Dallacasa, D., Orfei, A., et al. 2001, *A&A*, 379, 755

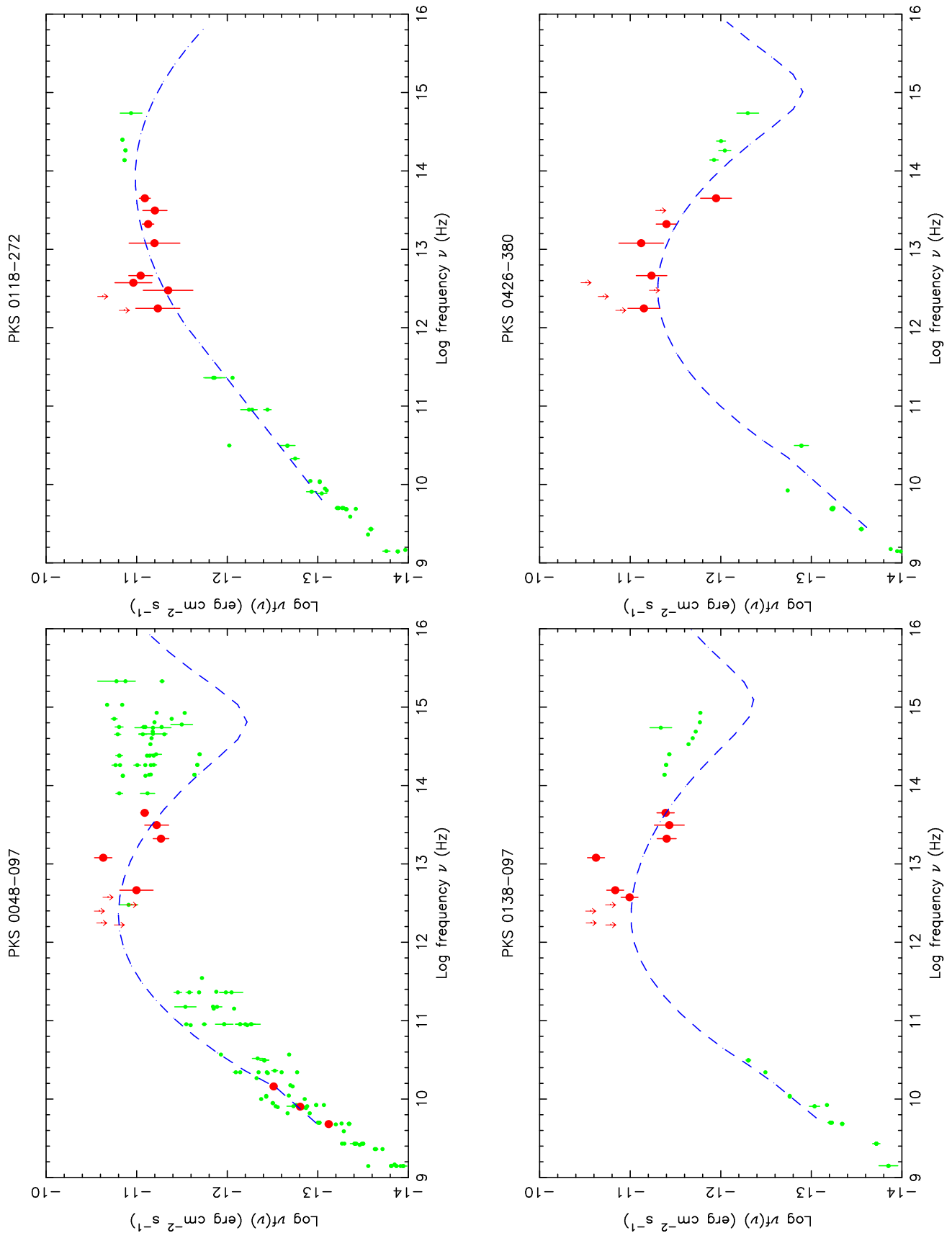


Fig. 1. The spectral energy distributions for our sources. Bigger, darker symbols indicate ISO data and the nearly-simultaneous radio (and optical in the case of PKS 0735+178, OQ 530, S5 1803+784, and S5 2007+777) data (arrows denote ISO upper limits), while smaller, lighter symbols represent non-simultaneous data collected from the literature. The dashed line is our synchrotron model.

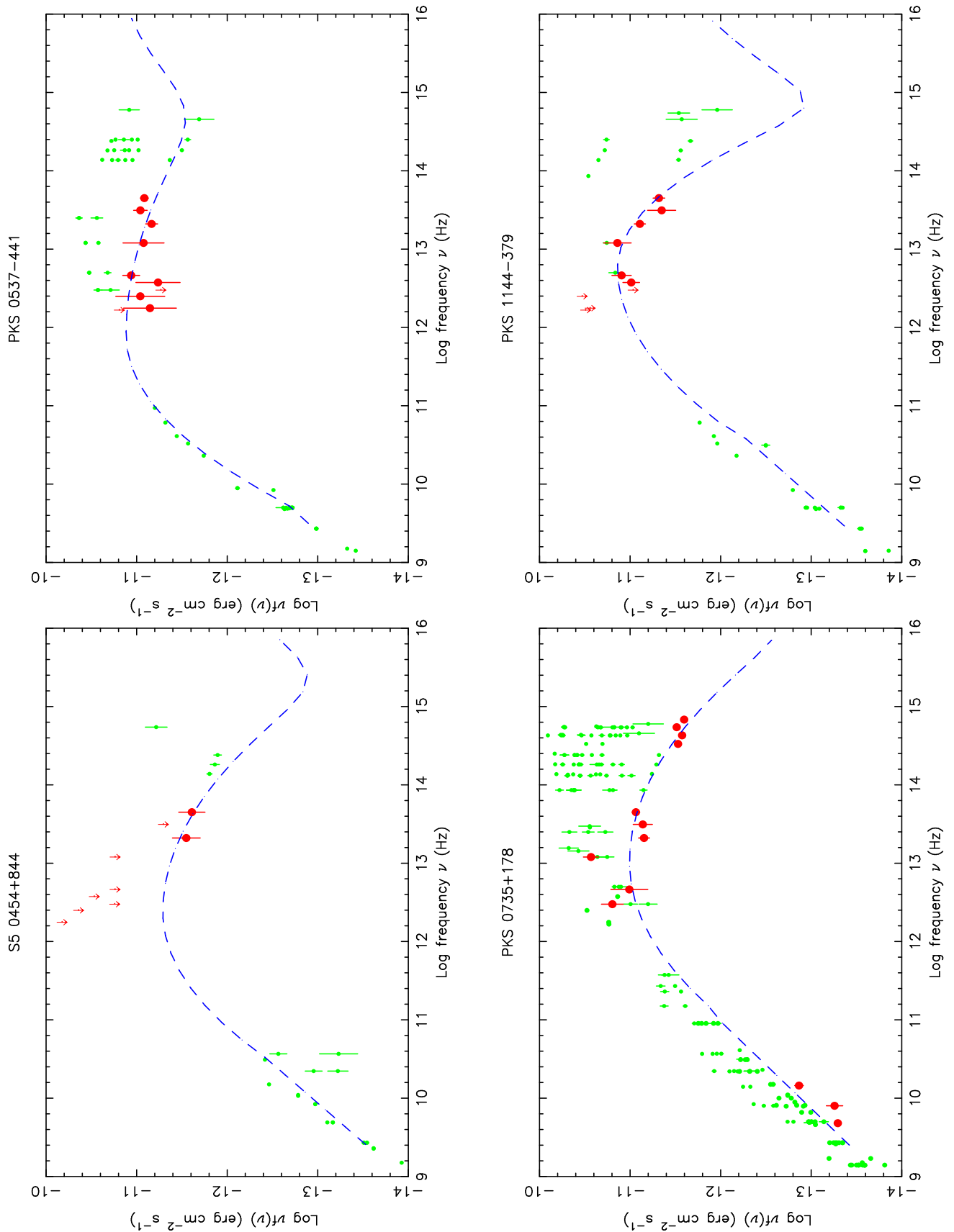


Fig. 1. (continued) The spectral energy distributions for our sources. Bigger, darker symbols indicate ISO data and the nearly-simultaneous radio (and optical in the case of PKS 0735+178, OQ 530, S5 1803+784, and S5 2007+777) data (arrows denote ISO upper limits), while smaller, lighter symbols represent non-simultaneous data collected from the literature. The dashed line is our synchrotron model.

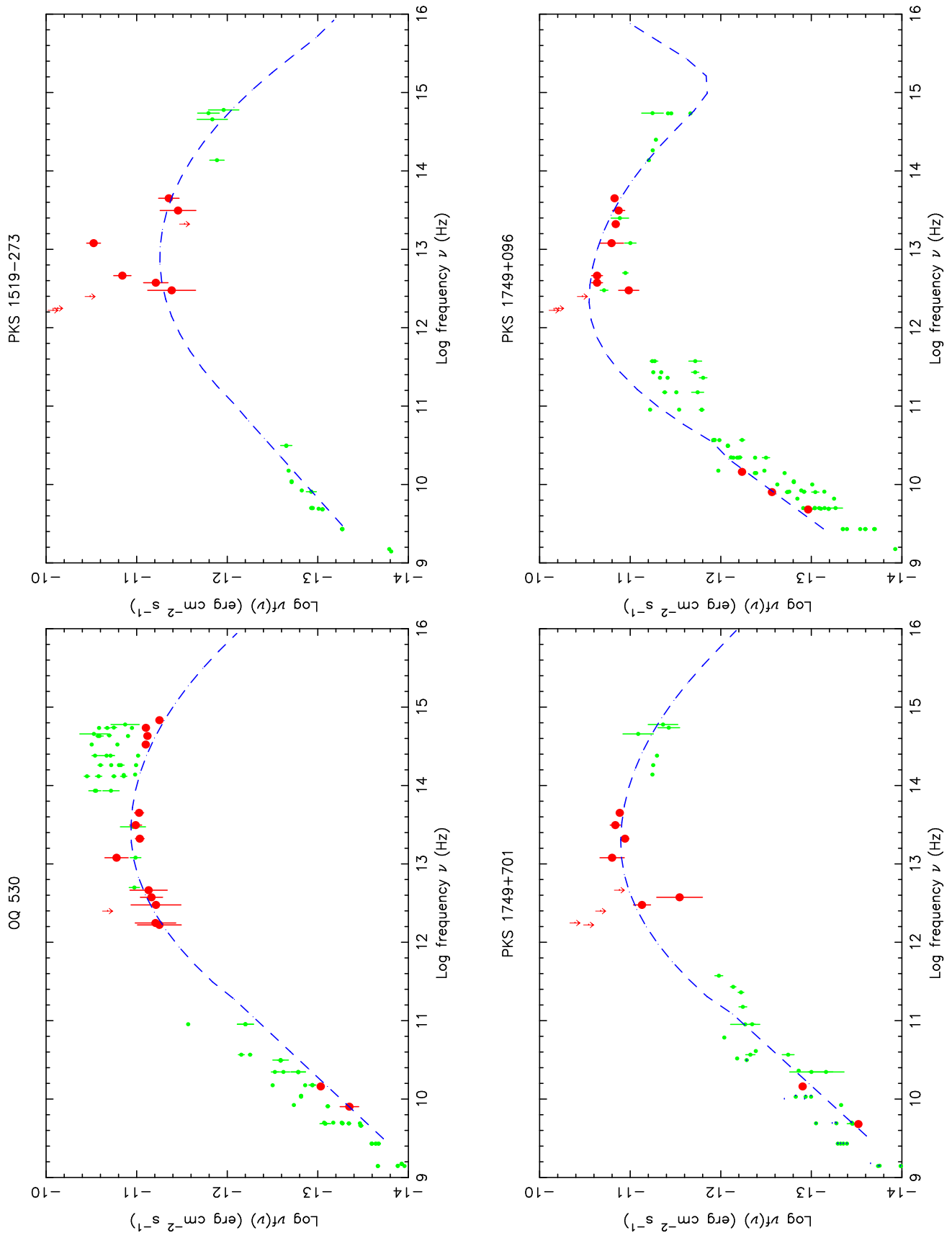


Fig. 1. (continued) The spectral energy distributions for our sources. Bigger, darker symbols indicate ISO data and the nearly-simultaneous radio (and optical in the case of PKS 0735+178, OQ 530, S5 1803+784, and S5 2007+777) data (arrows denote ISO upper limits), while smaller, lighter symbols represent non-simultaneous data collected from the literature. The dashed line is our synchrotron model.

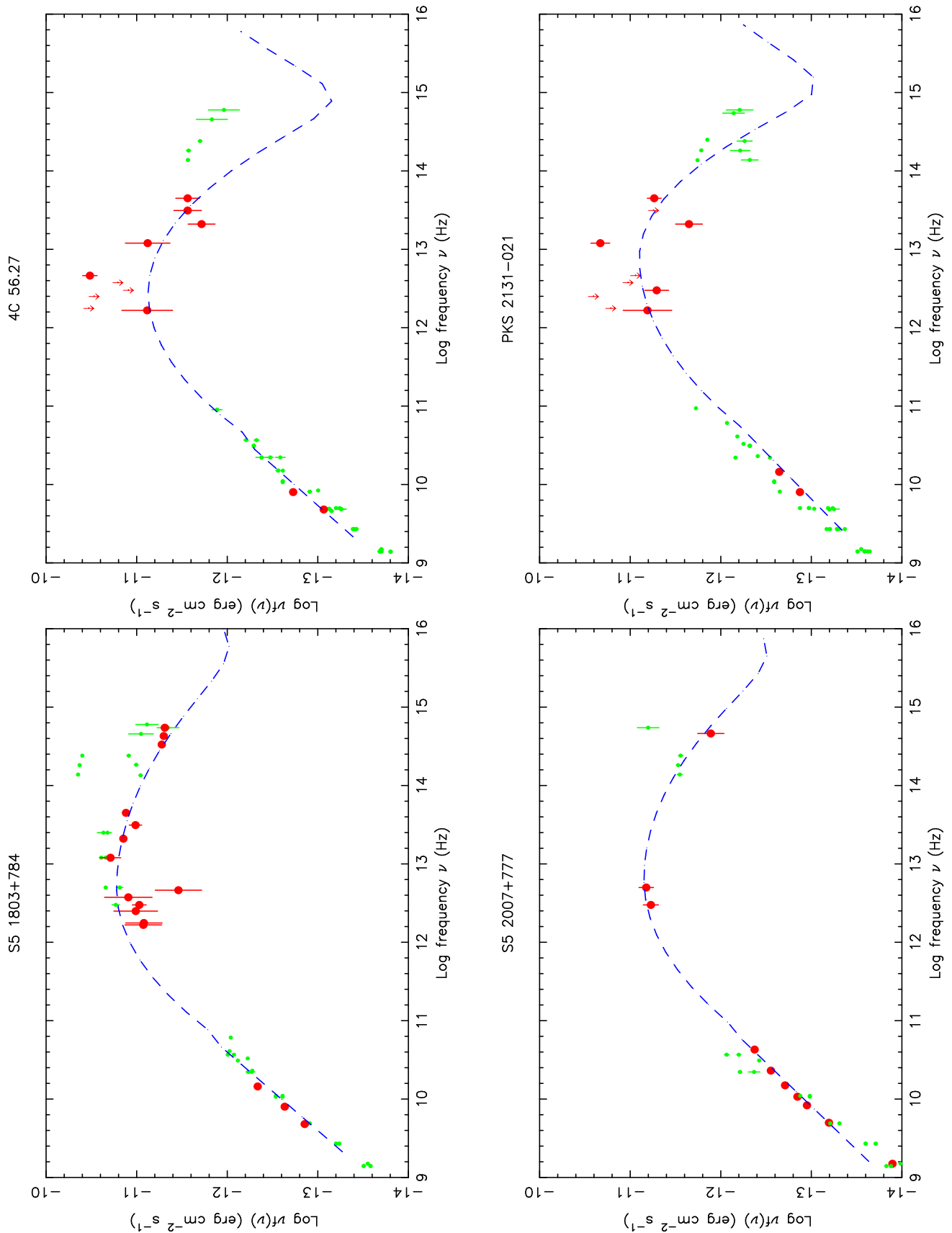


Fig. 1. (continued) The spectral energy distributions for our sources. Bigger, darker symbols indicate ISO data and the nearly-simultaneous radio (and optical in the case of PKS 0735+178, OQ 530, S5 1803+784, and S5 2007+777) data (arrows denote ISO upper limits), while smaller, lighter symbols represent non-simultaneous data collected from the literature. The dashed line is our synchrotron model.

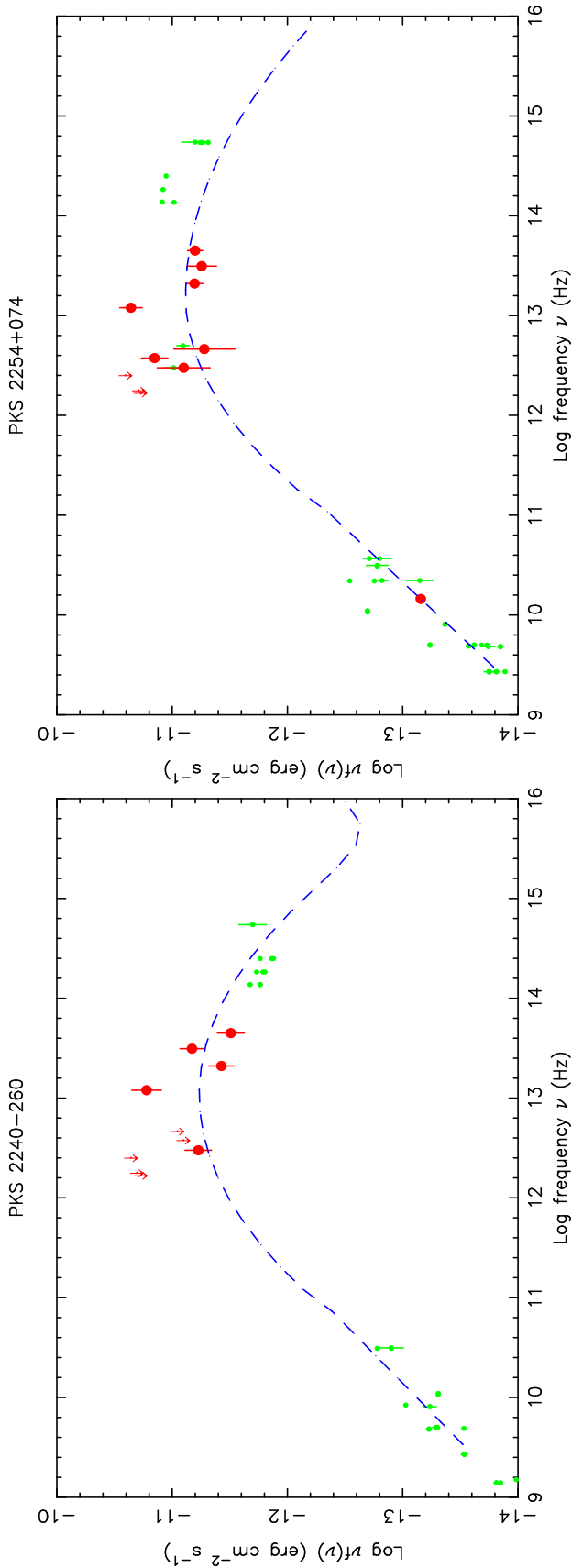


Fig. 1. (continued) The spectral energy distributions for our sources. Bigger, darker symbols indicate ISO data and the nearly-simultaneous radio (and optical in the case of PKS 0735+178, OQ 530, S5 1803+784, and S5 2007+777) data (arrows denote ISO upper limits), while smaller, lighter symbols represent non-simultaneous data collected from the literature. The dashed line is our synchrotron model.